The Point Cloud Visualisation For Rotary Optical Rangefinders

Pavel Chmelar, Ladislav Beran, Lubos Rejfek, Natalija Chmelarova
Department of electrical engineering
Faculty of electrical engineering and informatics
Pardubice, Czech Republic
pavel.chmelar@student.upce.cz, ladislav.beran@student.upce.cz, lubos.rejfek@student.upce.cz
nataliia.kudriavtseva@gmail.com

***Abstract*—This paper describes the point cloud visualization for rotary optical rangefinders. Measured distance data with image information from captured frames give a possibility to create a colored point cloud. The distance is measured by the vertical laser line and to select a color value directly from an actual measured frame is not possible. For this reason, the previous measurement frame is used. The individual frames shifting is estimated by the temple matching algorithm. The purpose of the paper is to show how easily it is possible to combine measurement data with image information in case of a color point cloud construction. The paper includes several examples of different point clouds to verify the algorithm's ability.**

Keywords—point cloud; template matching; rotary optical rangefinder; laser measurement; point cloud library

I. INTRODUCTION

The point cloud visualization is a method how to present measurement data more interactively. Its monotone visualization by a single color allows to present visual space features and an overall view, but there is missing a real visual form. From this reason have been developed many visualization methods which are implemented in several specialized libraries and software products.

The most recent library for a point cloud data processing and a visualization is the Point Cloud Library (PCL), presented in [1]. It is still actively developed and often used by many researches. The library contains state of the art algorithms for: filtering; feature estimation; surface reconstruction; registration; visualization; model fitting and segmentation. Also in this paper the achieved results are visualized by using this library. In comparison with the Matlab the PCL provides a faster processing speed from its nature.

The modern GPUs help with the accelerating visualization process [2]. The OpenGL API is supported by many platforms [1], [2] and especially for a big data sets visualization it is necessary to use the GPU power in case of the normal response preservation to the user, which analyses these data.

A good example of a point cloud visualization is the application with a drone [3]. Its task is the space mapping by the Ladar sensor and the visualization is used mainly for target distinguishing. The surrounding is presented in white and the potential target is colored. With the similar visualization importance dealing the research focused on the coal mines scanning [4]. Important scanned space features are distinguished by different colors. The connection with other sensors offers to assign parts with a different temperature or a gas concentration by a specific color. The depth information can be also expressed in colors.

Another interesting research is a point cloud connection with real textures for the street-view web navigation [5]. Authors offer real-time projective texturing on meshes and point clouds with an occlusion handling. Results look impressive and more three-dimensional than nowadays used approaches. A similar research [6] deals with large-scale point clouds in general. It is focused on representation for the visualization of large-scale point clouds accompanied by a set of high-resolution photographs. The result is a point cloud which looks like the real scene. The next research focuses on the detail documentation of a building construction [7]. The effort is to record the whole building construction including the processing and the visualization on computer. The research includes good achieved practical results.

The point cloud visualization is nowadays a favorite task for many researchers, especially by using the low-cost Microsoft Kinect sensor. In the paper [8] it is presented the Kinect sensor fusion with a time-of-flight camera (TOF) and LiDAR sensor. The research deals with the point cloud registration and the sensors' data fusion. The resulting point cloud is colored and the system is capable to meet with the requirements of indoor mapping, modeling, robot localization and navigation. The another robotic system equipped by a photovoltaic panel and designed for the cleaning uses the Kinect sensor for a 3D mapping including a visualization in large scale areas [9]. Similar to the previous researches the mobile robot for the unknown environment scanning is also equipped by the Kinect [10]. Furthermore, the robot uses OctoMap to store a created 3D map of an octree representation, which offers an efficient data structure for the robot navigation.

The Kinect is often used also in a health care to track a patient motion [11]. The system is able to create a 3D patient model. The 3D visualization is also important for the heart reconstruction from a point cloud [12]. In [13] it is presented a 3D mapping system for the indoor scanning with visual information. The recent research [14] focusses on a sophisticated data processing, a modelling and a data

The research was supported by the Internal Grant Agency of University of Pardubice, the project No. SGS_2017_030

visualization. This research aims for a volumetric, a parametric building model, that additionally incorporates contextual information such as a global wall connectivity.

The presented rotary optical rangefinder is described in [15] and [16]. In our previous research [17] we introduced the new modeling of a colored laser line by using the Gaussian Mixture Model (GMM). The new model is able to detect a laser color more precisely, to deal with a different laser intensity in an image, even eliminate a laser saturation phenomenon or investigate a presence of an ambient daylight. The next paper [18] presented the algorithm of a detail laser mask analysis. The new algorithm increasing mainly the number of measurement points and the precision. It also improves the green objects false detections, it is able to deal with a wider segmented green object and a distance detection on split segmented parts. One of the last research [19] deals with the depth map construction from any point clouds with any camera position and an orientation. The constructed depth map will give us more information about an object's and a space depth. The known pixel size information allows to measure physical dimensions.

This paper deals with a color point cloud representation which completing our autonomous optical rangefinder features. The rest of the paper is organized as follows. The Section 2. describes the rotary optical rangefinder and a 3D point cloud construction. The Section 3. deals with a color selection on measurement positions by using template matching algorithm. In section IV. are evaluated results. The paper ends by the conclusion and the evaluation of algorithm's abilities.

II. Rotary Optical Rangefinder

The 3D range scanning system for autonomous mapping, see Fig. 1, is based on the triangulation method. The principle of a distance determination and the 3D vector map construction is introduced in the paper [16].

Fig. 1. The rotary 3D range scanning system

The whole measuring device is pivotally carried by tripod. For image capturing a high-quality color camera with a resolution of 2590x1942 pixels is used. The used laser diode has an output power 200 mW, especially for good recognition after vertical swapping. The laser spot is dispersed by an optical filter with an angle of 90 degrees. The 360 degrees rotation of the measuring head provides a powerful and fast stepping motor. The measurement system is able to determine the vertical laser line with a half pixel accuracy. The whole system accuracy depends non-linearly on the measured distance, see [15] for more details.

A. Distance Determination

The Fig. 2 gives measurement results for one frame. The laser line is segmented by the GMM for a green colored laser. The laser beam is reflected from different surfaces with a variable intensity. The GMM model is appropriate for this task. Its segmentation mask is depicted in Fig. 3. The whole segmentation principle is described in our previous work [17].

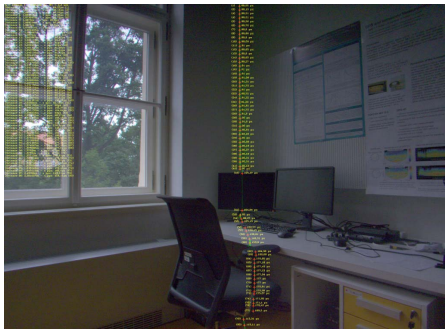

Fig. 2. One measurement frame example

Fig. 3. The segmentation mask for a measurement frame

The segmentation mask itself do not provide the exact information about the precise laser position. Even in Fig. 3 the left-top segmentation mask corner contains segmented green leaves of outside tree. For the final distance estimation, the detail laser line analysis is used. Our previous paper [18] shows how to estimate the best laser position. The presented algorithm also includes how to deal with parallel, reflected and wide laser lines and a laser colored objects detection. By the laser mask analysis were measured 68 different distances in Fig. 2 and the total measurement points N in one frame is 80.

The point cloud color visualisation is based mainly on the distance determination principle. This is the reason why it is described the complete detailed point cloud construction algorithm in this paper. The triangulation method is used for distance measurement. The principle is based on the triangle similarity. The Fig. 4 shows the basic distance determination principle. The illustration is depicted as a horizontal camera section. As in Fig. 1 there is a camera and a laser with the determined distance h between them. The point in the measurement distance D is the one of the vertical laser line points from Fig. 2.

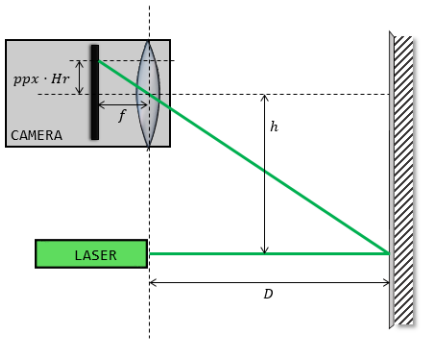

Fig. 4. The distance measurement principle (the horizontal section)

For the distance D calculation are used these parameters: f the focal length; h the distance between camera and the laser emitter. The laser is placed in the horizontal camera plane in this example; ppx the pixel offset from the centre of the image.

The listed parameters above have physical dimension in metrical units, only the ppx offset is a simple pixel count from the image centre. To express the ppx in the metrical units the knowledge of the camera sensor pixel size, denoted as Hr, is needed. The first triangle consists from a camera, a laser and the measurement distance D. The second triangle is behind the camera lens. It is created by the lens focal length f, the ppx offset and the reflected laser beam on the camera sensor. The relation between both triangles is defined as

$$\frac{h}{D} = \frac{ppx \cdot Hr}{f}. \tag{1}$$

The both triangle tangent angles are equal. The final distance determination equation is expressed from (1) as

$$D = \frac{h \cdot f}{Hr \cdot ppx}[m]. \tag{2}$$

The equation (2) plays important role in the point cloud construction, because its utilization is not only for distance determination but also it is used for the height expression.

B. Point Cloud Map Creation

The basics point cloud construction is presented in [16]. From this previous research the rotary optical rangefinder was significantly improved. Not only the hardware part, but mainly the data processing is enhanced. The color laser modelling by GMM [17] and the detail laser mask analysis [18] increased the measurement precision and maximize the measurement points amount.

The mobile platform is placed in a measured space on the position marked as

$$P = (P_X, P_Y, P_Z) \tag{3}$$

Indexes X, Y, Z are space coordinates. The point P is the origin for the automatic 360 degrees scan. For the point cloud construction it is necessary to select the appropriate coordinate system, where individual measurement points are stored. The Cartesian coordinate system was selected from its natural basics. Each point in a point cloud is presented as 3D vector

$$p = (p_x, p_y, p_z) \tag{4}$$

where p_x, p_y and p_z are coordinates in appropriate axis X, Y and Z. The initial platform position (3) is used for the appropriate point cloud placement in a space. The other important parameters are: the actual measuring head rotation angle φ_k; the measured distance $D_{i,k}$ in k-th angle step; the index i determinates the measurement position in height, its value range is $[0, 1, ..., N - 1]$; the parameter N is the number of measurement points.

The following illustration Fig. 5 gives the scanning direction.

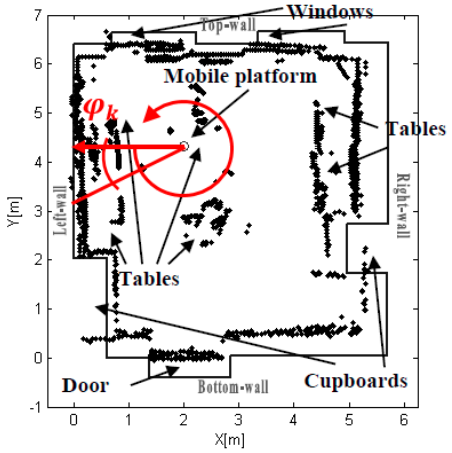

Fig. 5. The room top-view with the scanning ilustration

The marked angle step size φ_k is relatively small in real, but for the better illustration is depicted with bigger size in Fig. 5.

The measurement point p_x and p_y coordinates in the final point cloud are calculated as

$$p_{x,i} = P_x - \cos(\varphi_k) \cdot D_{i,k}, \quad p_{y,i} = P_y - \sin(\varphi_k) \cdot D_{i,k} \tag{5}$$

The angle steps number K is equal to count of steps which requires the measuring head for complete rotation during the measurement process. The k index range is $[1, 2, ..., K]$. The actual measurement angle φ_k in the measurement process is

$$\varphi_k = \frac{360°}{K} \cdot k \tag{6}$$

From equation (5) point's positions in plane are calculated and for the real 3D point it is necessary to express also

the p_z coordinate. The coordinate p_z is evaluated from several steps and the first is to get the point's *ppx* parameter.

$$ppx_{i,k} = \frac{h \cdot f}{D_{i,k} \cdot H_r} \tag{7}$$

The value h is known and with the knowledge of the *ppx* parameter the "the pixel length" $l_{pxDi,k}$ can be expressed as

$$l_{pxDi,k} = \frac{h}{ppx_{i,k}}. \tag{8}$$

The parameter $l_{pxDi,k}$ allows to measure a size by the pixel counts in a captured frame. The size measurement is a valid for an object at the same distance as the measured point $D_{i,k}$.

And finally the point's z coordinate is expressed from (8) and x pixel position (position on the laser line) on the captured frame

$$p_{z,i} = l_{pxDi,k} \cdot x_{i,k}. \tag{9}$$

Several created point clouds are shown in the Section 4 with results. There is also illustration with the colored and the normal point cloud.

III. Point Cloud Color Information

The color information is extracted from captured frames. Pixel values on measurement point's positions are extracted and stored for the color visualization. The direct color extraction from the actual measurement frame is not possible, because the laser beam covers the measurement position. Next illustration, see Fig. 6, shows 6 measurement frames joined into one frame.

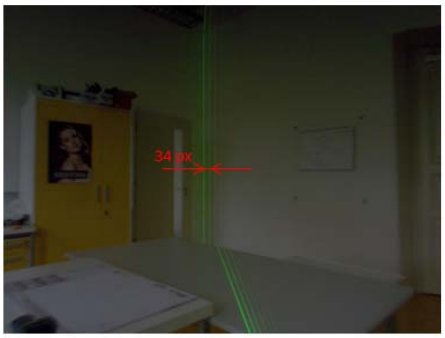

Fig. 6. The six measurement frames joined into one image

This group demonstrates the laser line movement during the measurement process. There are K measurement frames. The measurement process starts by the first frame and continues with others till all frames are processed. When the actual frame is processed the measurement positions for the previous frames are already known. The actual frame contains color information of the previous. For the last measurement frame as template the first measurement frame is used. To get these pixel's colors the shift information between the actual and previous frame is needed. The template matching algorithm is appropriate for this case. In Fig. 6 is illustrated the pixel shift 34px between two frames. This is a valid for a frame width 2590px during the 360 degrees scanning with the one angle step. The pixel shift $\Delta_{k,k+1}$ between two frames is the same, but it is better to use the precise algorithm to ensure the exact pixel shift between two frames.

The corresponding color point $c_{p(x,y,z)}$ information for the measurement position on the actual frame gives the following equation

$$c_{p(x,y,z)} = I_{k+1}(x_{i,k}, ppx_{i,k} + \Delta_{k,k+1}) \tag{10}$$

where $\Delta_{k,k+1}$ is the actual shift between k-th and $k+1$-th measurement frames, I_{k+1} is the next measurement frame. Other parameters are known from previous equations (7) and (9).

The three template matching operators were compared for this task [20]. The operator's requirement is the independence on the edge detection application, because the edges on captured frames are not considerable. As the first operator was tested SAD (Sum of Absolute Differences)

$$SAD(I,T) = \sum_{x,y} \left| I(x,y) - T(x,y) \right| \tag{11}$$

where I is the captured frame and T is the template. The indexes x and y are pixel positions. In SAD accumulator the minimum shows the template position. As a second operator was used simple 2D correlation defined as

$$r(I,T) = \frac{\sum_{x,y}(I_{x,y} - \mu_I) \cdot (T_{x,y} - \mu_T)}{\sqrt{\sum_{x,y}(I_{x,y} - \mu_I)^2 \cdot \sum_{x,y}(T_{x,y} - \mu_T)^2}} \tag{12}$$

where μ is the mean value of an image or a template. The last operator is Normalized 2D Cross Correlation defined as

$$Rn(u,v) = \frac{\sum_{x,y}(I_{x,y} - \overline{I_{u,v}}) \cdot (T_{x-u,y-v} - \overline{T})}{\sqrt{\sum_{x,y}(I_{x,y} - \overline{I_{u,v}})^2 \cdot \sum_{x,y}(T_{x-u,y-v} - \overline{T})^2}} \tag{13}$$

where u and v are crossed indexes, the I and the T with a line above are normalized objects. In both correlation accumulators the maximum shows the template position.

All operators give the same results but as the final operator is selected Normalized 2D Cross Correlation because of its processing speed. The Tab. 1 gives the operators' properties comparison.

TABLE I. TEMPLATE MATCHING METHODS COMPARISON

Method	*Processing speed*	*Edge independence*	*Searching point*
SAD	slow	true	min
Corr 2D	slow	true	max
NXCorr 2D	fast	true	max

The Fig. 7 shows the correlation accumulator with the marked maximum value and the Fig. 8. shows the template (a), taken from the left part of the previous image and the actual measurement frame (b)

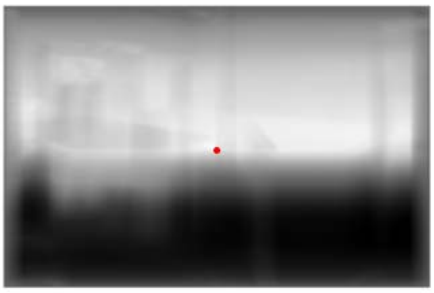

Fig. 7. The Normalised Cross Correlation accumulator with the marked maximum

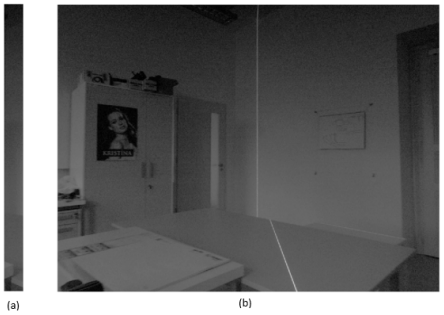

Fig. 8. The measurement frame (b) and the template (a)

During the scanning process there can be some undesired situations like some objects or spaces with a low variability of a pixel intensity or a measurement during the night or a measurement of some dark places. In these situations, template matching algorithms fail in the shift estimation between two measurement frames. In this case the standard shift value has to be used. This value deepens on the rotary rangefinder settings.

IV. RESULTS

The algorithm was verified on several point clouds, see Fig. 9. normal point cloud without color information, Fig. 10 the same point cloud with colors. The Fig. 11, Fig. 12, The Fig. 13 and Fig. 14 are next examples of indoor point clouds. The Fig. 10, Fig. 11 and Fig. 14 are indoor room scans and the Fig. 12 and Fig. 13 contains corridor point clouds.

All presented point clouds are visualized by using the Point Cloud Library, see [1]. The point's size is set to bigger, because the resulting point clouds look more compact.

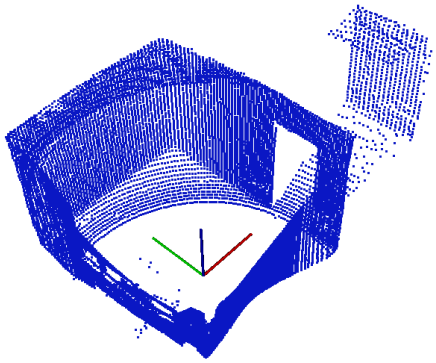

Fig. 9. The point cloud of a room without color information

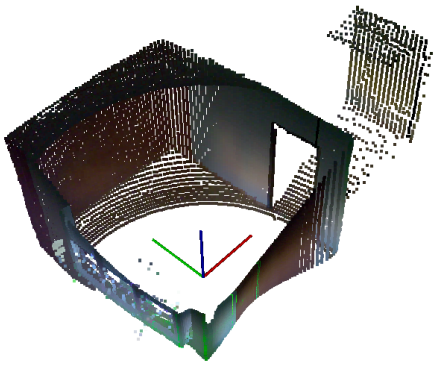

Fig. 10. The point cloud of a room with color information

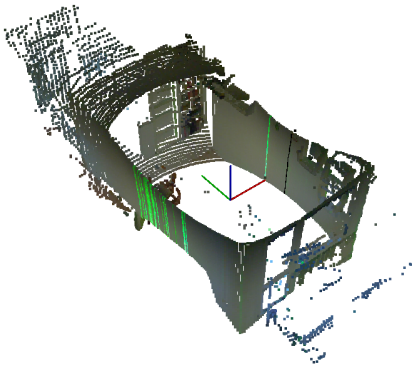

Fig. 11. The colored point cloud example of a room

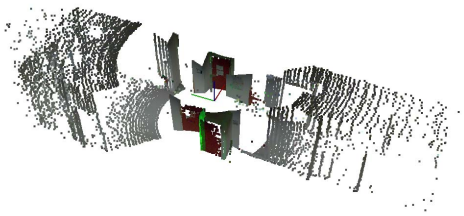

Fig. 12. The colored point cloud example of a coridor

During the pixel shift evaluation between two frame it is possible to notice, that in some situations the template

matching algorithm fails and in some point clouds are uncorrected color points. It is obvious from Fig. 10, Fig. 11, Fig. 12 and Fig. 14. In these point clouds remains traces of the vertical laser line. The problematic cases are caused by a low pixel variability especially on walls or same colored objects. These error estimations impairing the resulting point cloud a little, but in global it is not significant visual error.

On the resulting point clouds can be also applied the gamma correction especially in measurement of dark places. This ensures the improvement of the global appearance.

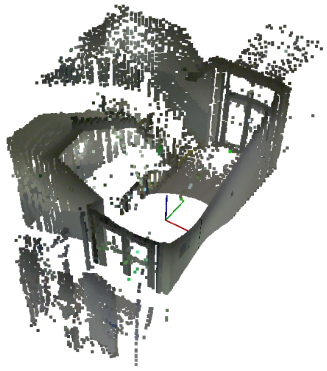

Fig. 13. The colored point cloud coridor with the stairs

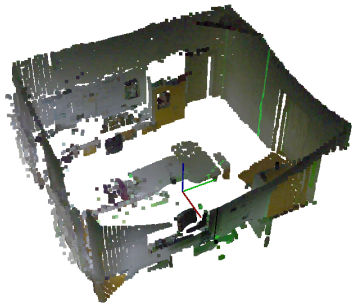

Fig. 14. The room colored point cloud

V. Conclusion

The paper describes the method how to get color information into point clouds created by rotary optical rangefinders. The color information serves only as the point cloud visualization. It is also nicer presentation of measurement data. Color information can be mainly important for architects but it finds usability in many research areas. We presented this solution also as an alternative to expensive rangefinders. Our rotary rangefinder consists only form a camera, a laser and a stepper motor.

The results show the algorithm's ability but in bigger distances the point density is smaller. Template matching algorithms lack also in situations with a small variability of pixel intensity like a white wall. This leads to some uncorrected points' color in resulting point clouds. The presented point clouds are measurements from a one place. To get more complex point clouds it is necessary to process more measurements from different places and use registration methods. Our future work will be focused on this.

References

[1] R. B. Rusu, and S. Cousins, "3D is here: Point cloud library (PCL)," 2011 IEEE International Conference on Robotics and Automation, Shanghai, 2011, pp. 1-4.

[2] C. H. Lo. Raymond, and C. Y. Lo. William, "OpenGL data visualization cookbook," Packt Publishing, August 2015.

[3] L. P. Berge, N. Aouf, T. Duval, and G. Coppin, "Generation and VR visualization of 3D point clouds for drone target validation assisted by an operator," 2016 8th Computer Science and Electronic Engineering (CEEC), Colchester, 2016, pp. 66-70.

[4] T. Kot, P. Novak, and J. Babjak, "Visualization of point clouds built from 3D scanning in coal mines," 2016 17th International Carpathian Control Conference (ICCC), Tatranska Lomnica, 2016, pp. 372-377.

[5] A. Devaux, and M. Bredif, "Realtime projective multi-texturing of point clouds and meshes for a realistic street-view web navigation," In Proceedings of the 21st International Conference on Web3D Technology (Web3D '16), ACM, New York, NY, USA, 105-108.

[6] M. Arikan, R. Preiner, C. Scheiblauer, S. Jeschke, and M. Wimmer, "Large-scale point-cloud visualization through localized textured surface reconstruction," in IEEE Transactions on Visualization and Computer Graphics, vol. 20, no. 9, pp. 1280-1292, Sept. 2014.

[7] K. K. Han, and M. Golparvar-Fard, "Potential of big visual data and building information modeling for construction performance analytics: An exploratory study," Automation in Construction, Volume 73, January 2017, Pages 184-198.

[8] C. Chen, B. S. Yang, and S. Song, "Low cost and efficient 3D indoor mapping using multiple consumer RGB-D cameras," International Archives of the Photogrammetry, Remote Sensing and Spatial Information Sciences - ISPRS Archives, 2016-January, pp. 169-174.

[9] M. Li, M. Zhang, Y. Fu, W. Guo, X. Zhong, X. Wang, and F. Chen, "Fast and robust mapping with low-cost Kinect V2 for photovoltaic panel cleaning robot," 2016 International Conference on Advanced Robotics and Mechatronics (ICARM), Macau, 2016, pp. 95-100.

[10] J. W. Li, D. F. Zheng, Z. H. Guan, C. Y. Chen, X. W. Jiang, and X. H. Zhang, "Indoor 3D scene reconstruction for mobile robots using Microsoft kinect sensor," 2016 35th Chinese Control Conference (CCC), Chengdu, 2016, pp. 6324-6328.

[11] N. L. Dao, Y. Zhang, J. Zheng, and J. Cai, "Kinect-based non-intrusive human gait analysis and visualization," 2015 IEEE 17th International Workshop on Multimedia Signal Processing (MMSP), Xiamen, 2015, pp. 1-6.

[12] J. Li, X. Ma, Y. Jia, and X. Zhou, "3D visualization for heart model from point clouds," 2012 International Conference on Audio, Language and Image Processing, Shanghai, 2012, pp. 1077-1081.

[13] J. Chen, and Y. K. Cho, "Real-time 3D mobile mapping for the built environment," ISARC 2016 - 33rd International Symposium on Automation and Robotics in Construction, pp. 226-233.

[14] S. Ochmann, R. Vock, R. Wessel, and R. Klein, "Automatic reconstruction of parametric building models from indoor point clouds," Computers & Graphics, Volume 54, February 2016, Pages 94-103

[15] P. Chmelar, and M. Dobrovolny, "The optical measuring device for the autonomous exploration and mapping of unknown environments," Perner´s Contacts, 2012, vol. VII, no. 4,pp. 41-50.

[16] P. Chmelar, and M. Dobrovolny, "The fusion of ultrasonic and optical measurement devices for autonomous mapping," Radioelektronika 23rd International Conference, 2013

[17] P. Chmelar, L. Beran, and N. Kudriavtseva, "The Laser Color Detection for 3D Range Scanning Using Gaussian Mixture Model," Radioelektronika, 25th International Conference, 2015

[18] N. Chmelarova, P. Chmelar, L. Beran, and L. Rejfek, "Improving precision of laser line detection in 3D range scanning systems," 2016 26th International Conference Radioelektronika, Kosice, 2016, pp. 207-212.

[19] P. Chmelar, L. Beran, and L. Rejfek, "The depth map construction from a 3D Point Cloud" MATEC Web Conf., 75, 2016.

[20] C. R. Gonzalez, E. R. Woods, and L. S. Eddins, "Digital image processing using MATLAB," 2nd ed., 2009 Gastemark, LLC.